Available online at www.sciencedirect.com
ScienceDirect
International Journal of Rock Mechanics & Mining Sciences 45 (2008) 1320–1334
International Journal of Rock Mechanics and Mining Sciences
www.elsevier.com/locate/ijrmms

Stress effects on permeability in a fractured rock mass with correlated fracture length and aperture

Alireza Baghbanan*, Lanru Jing

Engineering Geology and Geophysics Research Group, Royal Institute of Technology (KTH), Stockholm, Sweden

Received 25 June 2007; received in revised form 17 January 2008; accepted 27 January 2008
Available online 14 March 2008

Abstract

The effect of stress on permeability and fluid flow patterns in fractured rock masses is studied when distributed fracture aperture is correlated with fracture trace length, using a discrete element method (DEM). The basic assumptions are that the rock matrix is impermeable and linearly elastic, and that the fluid flows only in fractures. A new nonlinear algorithm is developed for prediction of normal stress–normal displacement behavior of fractures based on the Bandis model and the correlation between aperture and length. The results show that when small stress ratios (K = horizontal/vertical stress) are applied at the model boundaries, the overall permeability of the fracture network is generally decreased. However, contribution from a few large fractures of higher hydraulic conductivity prevents drastic reduction of the overall permeability, compared with models that assume uniform fracture apertures. With large values of the stress ratio, both the overall permeability and flow patterns are controlled by a combination of highly conductive larger fractures and fractures with shear slipping and dilation, with much increased overall permeability and shear-induced flow channeling. With increasing stress ratios, it becomes more and more difficult to establish an equivalent permeability tensor and representative elementary volume (REV) of a fractured rock, compared with the unstressed model. These results show significant difference between correlated and non-correlated aperture and fracture length distributions, and highlight more significant scale and stress dependence of hydro-mechanical behavior of fractures rocks when geometric parameters of rock fractures are correlated.

Keywords: Stress effect; Scale effect; Equivalent permeability tensor; Aperture–trace length correlation; Fracture rocks; Discrete fracture network; Deformability of fractures; Discrete element method

1. Introduction

Understanding the influence of stresses on overall permeability and flow pathways is very important for numerical modeling of the coupled hydro-mechanical process of fractured rocks in various fields of rock engineering, such as slopes, dam foundations, underground excavations, oil recovery, geothermal reservoirs and nuclear waste disposal [1]. In crystalline rocks where the permeability of the rock matrix may be negligible, flow occurs mainly through the connected fractures, or fracture networks. The overall permeability of the fracture network is influenced not only by characteristic geometric parameters of fracture systems, but also by states and evolutions of stress fields.

Fracture systems in rock masses are geometrically complex. The quality and quantities of measured data of geometric parameters, which are obtained from field mapping on exposed outcrops of limited areas and borehole logging of limited borehole diameters and depths, contains a large degree of uncertainty. To reduce such uncertainty in representing the subsurface fracture system more realistically, the usual practice is to use stochastic discrete fracture network (DFN) modeling by assuming that geometrical parameters of the fractures are statistically distributed [2]. The uncertainty in the geometric datasets can be reduced to a certain extent when a large number of DFN realizations, based on the probabilistic distribution functions of these parameters, are used as the geometric models for simulations of hydro-mechanical behavior of

*Corresponding author. Tel.: +46 8 790 6807; fax: +46 8 790 6810.
E-mail address: bagh110@kth.se (A. Baghbanan).

1365-1609/$ - see front matter © 2008 Elsevier Ltd. All rights reserved.
doi:10.1016/j.ijrmms.2008.01.015

fractured rocks. The flow in fractures is usually assumed to follow the cubic law, and the rock matrix is assumed to be impermeable. Equivalent permeability tensors may be derived when a representative elementary volume (REV) of the fracture system can be established and the stress effect on such equivalent DFN models can be studied using discrete element method (DEM). In the DEM models, the stress effects on fracture aperture evolutions can be considered by simulating processes of motion and deformation of the discrete blocks formed by the fractures, as reported in Refs. [3,4].

For studies about effect of stress on permeability tensor of fractured rocks as equivalent porous media, the key requirements are (a) the sizes of DFN model must not be less than the REV defined for evaluating the equivalent permeability tensor [3,5], (b) the constitutive model of fractures must include the non-linear normal stress–normal closure behavior of the rough rock fractures, such as the hyperbolic model by Bandis [6], and (c) the dilation of the fracture during shear must be non-zero in the fracture models.

In some earlier studies on stress effects on permeability of fractured rocks using DEM approach, such as [7–17], these requirements were not fully considered; either the REV issue was not addressed, constant normal stiffness of fractures were assumed, or zero dilation angles were used, which made the numerical model less suitable for studying stress-dependency of the hydraulic behavior of fractured rocks. A comprehensive study in Ref. [4] considered all three requirements as listed above and serves as a starting point for the further development of DEM models for stress and scale-dependent permeability of fractured rocks, considering correlation between fracture aperture and trace length [5].

Numerical results in Ref. [4] with constant aperture for fractures show stress-induced flow channeling and increased overall permeability of the fractured rocks. However hydro-mechanical study in the context of a performance assessment of deep waste disposal in the same site [18] also show a significant impact of using the spatial distribution of mechanical properties on deformability and hydraulic properties of fractured rocks, which means that the assumption of the constant hydraulic aperture of fractures as well as scale-independent mechanical behavior of fractures in the DEM models as reported in Ref. [4] need to be further investigated to consider both stress and scale-dependence in characterization of hydraulic apertures of fractures and equivalent permeability. The aim of this paper is to solve this problem.

Based on different fracture mapping results as reported in literature, fracture aperture appears to follow different distribution functions [5,19–26] and could be correlated with fracture trace length [5,27–29]. The numerical results in Ref. [5] demonstrate a significant increase of scale-dependency of the permeability of fractured rocks, when correlation between fracture aperture and trace length is considered. With increasing values of the second moment of a log-normal distribution of apertures, the DFN models show more discrete hydraulic behavior. Equivalent permeability tensors can be approximated only with smaller values of the second moments and with much larger REV sizes. The results also show that the assumption of constant aperture could lead to unknown uncertainties in the estimations of REV and equivalent permeability for fractured crystaline rocks.

The objective of this study is to evaluate the stress and scale effect on the existence of permeability tensor and change of flow pathways when initial fracture aperture is log-normally distributed and correlated with fracture trace length following a power law distribution. A non-linear behavior between normal stress–normal displacements of fractures is adopted so that both scale and stress-dependent normal stiffness of fractures can be considered. The computational model is based on a hydraulic REV of $20\,\mathrm{m} \times 20\,\mathrm{m}$ in size as derived with second moment of $b = 1$ and correlated with fracture trace length, as reported in Ref. [5], using a 2D DEM approach. The work represents a continuous research based on the fundamental approaches established in Refs. [4,5] but with more sophisticated characterization on the correlation between fracture aperture and trace length, and stress effects.

The 2D discrete element method code UDEC is used as the numerical tool for the fluid flow simulations and stress-effect studies, with the assumption that intact rock matrix is linear elastic and impermeable, and the fluid flows only through connected fractures obeying the cubic law [30].

In this paper, firstly a mathematical expression for the non-linear normal stress–normal displacement behavior for single fractures is developed; with the initial fracture apertures correlated with fracture trace lengths, so that the apertures and normal closures of the fractures are both scale- and stress-dependent. Fluid flow through the DFN models, which are at the REV size as determined in Ref. [5], is then simulated considering the effect of different stress boundary conditions, and its impact on permeability components, flow patterns and existence of an equivalent permeability tensor are evaluated.

2. Deformability of the single fractures with correlation between aperture and trace length

Laboratory studies of normal stress–normal displacement (changing in aperture) of rock fractures [31–38] show that the specific flow rate and hydraulic conductivity of fractures decrease or increase nonlinearly with increase or decrease of the normal stress during loading and unloading processes, respectively. On the other hand, the results of coupled shear-flow tests [38–42] show that in most cases the specific flow rate and hydraulic conductivity of a fracture increases with increasing shear displacement due to the shear dilation. In this section, a non-linear relation of the normal displacement-normal stress is developed when the initial fracture aperture is correlated with fracture trace

length so that both the closure and normal stiffness are trace length- and stress-dependent.

2.1. Mechanical behavior of fractures in the normal direction

The most widely adopted model for a nonlinear behavior of fracture under normal stress is the hyperbolic function for normal closure of fracture with respect to normal stress as reported in Refs. [6,32,33]. In Ref. [32], the fracture closure, δ, is related to the normal stress, σ_n, through an empirical hyperbolic relation:

$$\sigma_n = \sigma_{n0}\left[1 + \left(\frac{\delta}{\delta_m - \delta}\right)^t\right] \quad \text{for } \sigma_n \geqslant \sigma_{n0}. \tag{1}$$

The stress value of $\sigma_n = \sigma_{n0}$ is the initial normal stress or the so-called low seating normal stress, t is a dimensionless empirical exponent, and δ_m is the maximum possible fracture closure, approached asymptotically as the normal stress increases.

A more compact form of the hyperbolic relation fitting the fracture closure-normal stress behavior is reported in Ref. [33]:

$$\sigma_n = \frac{k_{n0}\delta}{1 - (\delta/\delta_m)} = \frac{k_{n0}\delta_m\delta}{\delta_m - \delta}, \tag{2}$$

where k_{n0} is an empirical parameter representing the initial normal stiffness. The fracture closure is related to normal stress by

$$\delta = \left(\frac{\sigma_n}{\sigma_n + k_{n0}\delta_m}\right)\delta_m \tag{3}$$

and the normal stiffness of fracture, k_n, is given by

$$k_n = \frac{d\sigma_n}{d\delta} = \frac{k_{n0}}{(1 - \delta/\delta_m)^2}, \tag{4}$$

where k_{n0} is the normal stiffness at a low confining stress. The function proposed in Ref. [32] reduces to Eq. (2) when $t = 1$ and $\sigma_n \gg \sigma_{n0}$. We can write Eq. (4) as a function of normal stress:

$$k_n = \frac{(\sigma_n + k_{n0}\delta_m)^2}{k_{n0}\delta_m^2}. \tag{5}$$

Efforts have been made to find initial normal stiffness, k_{n0} and maximum fracture closure, δ_m as functions of other fracture characteristic parameters. The Barton–Bandis empirical fracture constitutive model, such as reported in Ref. [43], is a relation between initial normal stiffness and maximum fracture closure, as a function of initial aperture, h_i, laboratory scale fracture wall compression strength, JCS_0, and laboratory scale fracture roughness coefficient, JRC_0 in the following forms,

$$k_{n0} = 0.0178\left[\frac{JCS_0}{h_i}\right] + 1.748JRC_0 - 7.155 \tag{6}$$

and

$$\delta_m = \alpha + \beta(JRC_0) + \gamma\left[\frac{JCS_0}{h_i}\right]^\eta, \tag{7}$$

where α, β, γ and η are empirical constants associated with normal loading cycle numbers during a cyclic loading–unloading normal compression tests of a rock fracture. These empirical equations and the associated constants are most valid in the tested samples under the specific testing conditions and processes, but cares need to be taken when they are applied to general practical problems.

Another approximate relation was proposed in Ref. [26] between hydraulic aperture and effective stress, but is based on the results of only one laboratory experiment. Therefore there may be difficulties for being extend to general behaviors of rock fractures.

Experimental studies about effect of stress on fracture permeability show that there may be an effect of sample size on fracture permeability [31,35]. The experimental results about the compressibility of rock fracture with different type of roughness also show that the maximum fracture closure is roughly proportional to the fracture length [35]. This means that the deformability of fractures under normal stress is also a function of fracture size, or trace lengths in 2D models.

In this study, based on Eq. (3), we develop an empirical equation for prediction of mechanical behavior of rock fractures in the direction normal to the mean fracture plane, when the initial hydraulic aperture is log-normally distributed and correlated with fracture trace length, and is calculated with variation of the normal closure δ of the fracture.

Eq. (3) might be rewritten as

$$\frac{\delta}{\delta_m} = \frac{\sigma_n}{\sigma_n + k_{n0}\delta_m} = \frac{\sigma_n}{\sigma_n + \sigma_{n0}} = \frac{\sigma_n/\sigma_{n0}}{(\sigma_n/\sigma_{n0}) + 1}, \tag{8}$$

where $\sigma_{n0} = k_{n0}\delta_m$.

Fig. 1 shows a schematic variation of normalized normal closure, δ/δ_m (represented by solid line) and relative normal compliance, C_n (represented by dashed line) that is calculated by

$$C_n = \frac{\partial(\delta/\delta_m)}{\partial(\sigma_n/\sigma_{n0})} = \frac{1}{(1 + \sigma_n/\sigma_{n0})^2} \tag{9}$$

versus normalized normal stress of rock fractures, σ_n/σ_{n0}, using Eqs. (8) and (9). It can be seen that when the normal stress ratio is large enough, the variations of the normalized closure and normal stresses become very small, and the normal closure approaches the maximum closure with a significant decrease of relative normal compliance.

Here for a purpose of demonstration, we assume that minimum variation of δ/δ_m is approximated when the values of δ/δ_m is beyond 0.9 (Fig. 1). Therefore, the corresponded normalized normal stresses exceed 9, according to Eq. (8). In this study this value defined as the normalized critical normal stress σ_{nc}/σ_{n0}, is assumed to be 10 (Fig. 1). At the critical normal stress, the normal

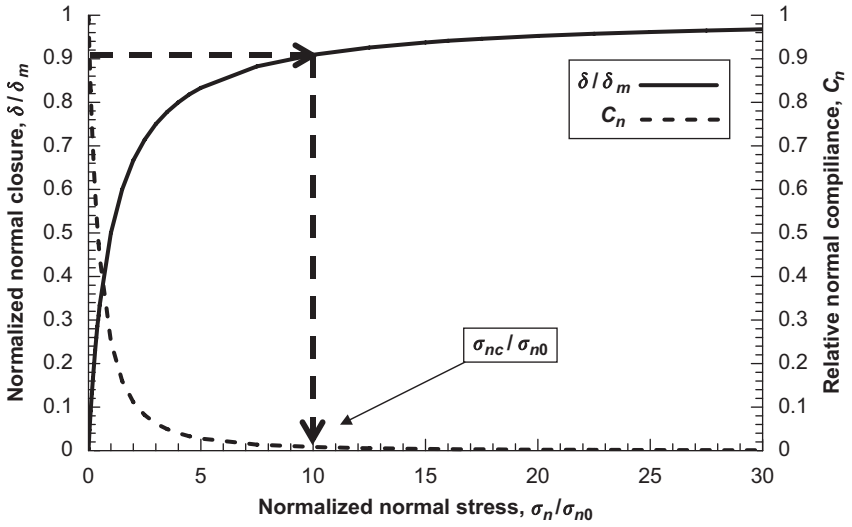

Fig. 1. Schematic variation of normalized normal closure, δ/δ_m and relative normal compliance, C_n, versus normalized normal stress of rock fractures, σ_n/σ_{n0}.

stiffness takes a form of $k_{n0} = \sigma_{nc}/10\delta_m$. Substitution of $k_{n0} = \sigma_{nc}/10\delta_m$ into Eq. (2) leads to a simplified normal stress–normal closure relation of

$$\sigma_n = \frac{\sigma_{nc}\delta}{10(\delta_m - \delta)}. \tag{10}$$

The normal stiffness is then associated with this stress–closure relationship given by

$$k_n = \frac{(10\sigma_n + \sigma_{nc})^2}{10\sigma_{nc}\delta_m}. \tag{11}$$

Fig. 2a–c shows the results of a sensitivity analysis on the effect of the ratio of maximum fracture closure with respect to the initial hydraulic aperture on fracture deformability when the critical normal stress is a constant, $\sigma_{nc} = 30$ MPa. In this example, the effects of three different initial aperture values $h_i = 10$, 65 and 200 μm are examined. The effect of variable critical normal stress when $\delta_m/h_i = 0.9$ is also illustrated in Fig. 2d–f.

With increasing ratio of the maximum fracture closure over the initial hydraulic aperture, normal stiffness decreases, and the variation of current aperture with normal stress becomes more significant (Figs. 2a–c). On the other hand, some experimental results of direct flow shear tests show that there is always a residual flow even at high normal stresses [31]. Therefore, the maximum fracture closure, which is to say the maximum residual aperture, is less than initial aperture, and it can be a function of initial aperture and should be determined by experiments [31,33]. In this study for simplicity, and also for detection of the effect of low applied normal stress on fracture aperture, we choose $\delta_m/h_i = 0.9$.

According to the model proposed above, the deformability of rock fractures is significantly affected by the normal stress. Observations of deformability characteristics with constant values of δ_m/h_i (Fig. 2d–f) illustrate that with increasing normal stress, fractures become stiffer. For fractures with small initial apertures when a large value of σ_{nc} is assumed, fractures maintain conductive even at high normal stresses. Therefore, the overall permeability of fracture networks increases when the fracture aperture is correlated with fracture trace length in DFN models containing some larger scale fractures. Experimental results have shown that with increasing initial hydraulic aperture (transmissivity), higher normal stresses have to be applied to reach the maximum normal closure of fractures [31–33].

As reported in Ref. [4], the critical normal stress is 30 MPa where the initial aperture is 65 μm for all of the fractures. There is as yet no practical technique to measure the deformability of large fractures in the field. Therefore, estimation of critical normal stress based on linearly proportional variations of fractures size was adopted in this study. The critical normal stress is assumed to vary between 3 and 100 MPa that is proportionally linear to a range of initial aperture from 1 to 200 μm taken from a previous study in Ref. [5].

Considering these assumptions and using Eqs. (10) and (11), the normal stress is related to the normal closure by

$$\sigma_n = \frac{\sigma_{nc}\delta}{10(0.9h_i - \delta)} \tag{12}$$

and the normal stiffness is linked to the normal stress as given by

$$k_n = \frac{(10\sigma_n + \sigma_{nc})^2}{9\sigma_{nc}h_i}, \tag{13}$$

where $\sigma_{nc}\,(\text{MPa}) = 0.487h_i\,(\mu\text{m}) + 2.51$.

Fig. 3 shows the variations of normal deformability of fractures under normal stresses for different initial hydraulic apertures. It can be seen that the normal deformation of fractures under small normal stresses is significant, even for fractures with small initial apertures.

In this study the initial hydraulic aperture is distributed log-normally and correlated with fracture trace

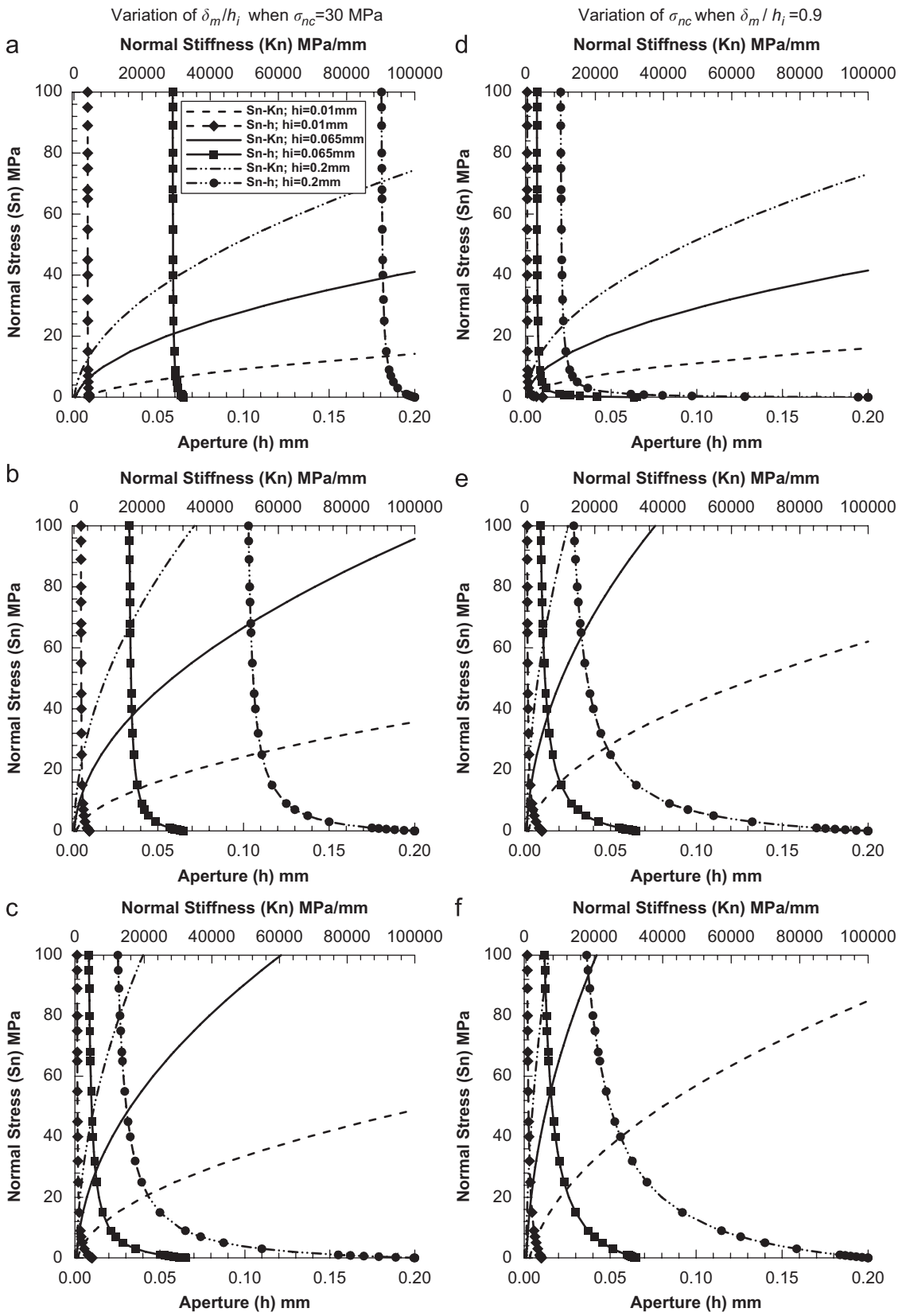

Fig. 2. Deformability characteristics of a fracture under normal stress when critical normal stress is constant and $\delta_m/h_i = 0.1$ (a), $\delta_m/h_i = 0.5$ (b), $\delta_m/h_i = 0.9$ (c), and the same analysis when the ratio of maximum fracture closure to initial aperture is constant and $\sigma_{nc} = 3$ MPa (d), $\sigma_{nc} = 50$ MPa (e), and $\sigma_{nc} = 100$ MPa (f).

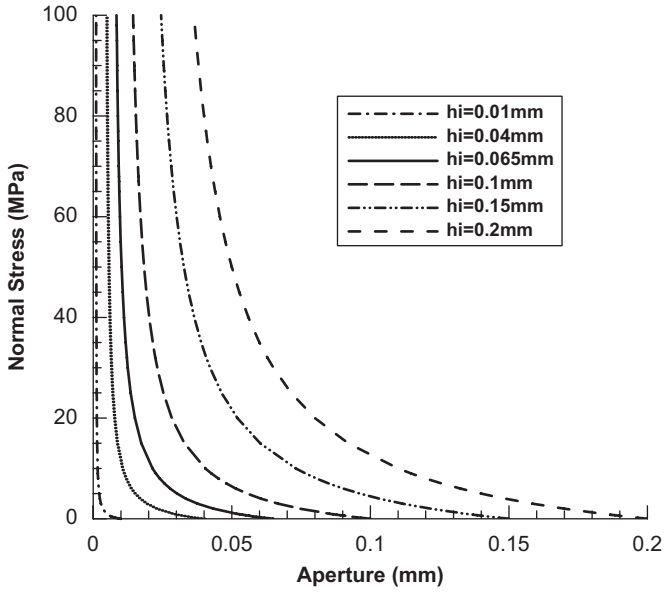

Fig. 3. Variation of aperture with normal stress for assumed initial apertures.

length by [5]:

$$l = \left\{ l_{\min}^{-D} + \left[\frac{g(h_i) - g(h_{ia})}{g(h_{ib}) - g(h_{ia})} \right] (l_{\max}^{-D} - l_{\min}^{-D}) \right\}^{-1/D}, \quad (14)$$

where $g(h_i) = \mathrm{erf}[(\mathrm{In}\, h_i - \bar{h}_{i\ \log})/\sqrt{2}b_i]$.

The terms $\bar{h}_{i\ \log}$ and b_i are the first and second moments of the log-normal distribution of initial apertures, respectively, and erf(x) is the error function of x. The symbols h_{ia} and h_{ib} represent the lower and upper initial aperture limits, $l_{\min}$ and $l_{\max}$ are the minimum and maximum trace lengths, and D is the fractal dimension. This equation represents a correlation relation between the fracture aperture and trace length, with the aperture following a truncated log-normal distribution, and the fracture trace length following a truncated power law distribution. When we substitute the stochastically generated aperture values from Eq. (14) into Eqs. (12) and (13), the deformability of each fracture in the fracture network becomes a function of fracture trace length. In this way, both the normal stress effect and effect of the fractures size are linked through the correlation relation (14). The effect of shear dilation on fracture aperture is considered separately in the constitutive models of the rock fractures in UDEC code.

2.2. Fracture shear behavior

Aside from the magnitudes of boundary stresses, orientations and friction angles of the fractures are significant for the stress states along and across the fractures. Shear failure occurs when created shear stress component is greater than shear resistance of each fracture, depending on the friction angle and fracture orientation relative to the applied boundary stresses. When there is only a single fracture, this problem can be analyzed with the aid of a Mohr diagram [44]. Numerical models such as DEM are needed to determine the stress states of fractures in fracture networks where fractures have finite sizes and interact with each other. Shear dilation occurs as a result of overriding asperities of two rough fracture surfaces, represented here by a dilation angle, and may reach to the stationary value with increasing the fracture shearing according to the constitutive model adopted. In this study, the shear stress–shear displacement behavior of fractures was modeled by an elasto-perfectly plastic constitutive model with a Mohr–Coulomb failure criterion and fracture dilation occurs when it starts to slide. This dilation continues until a pre-defined critical shear displacement value, beyond which the dilation stops [4,30]. Since the main objective of this work is to determine the effect of stress on the fracture network permeability when the normal deformability of fractures is scale and stress dependent, the asperity damage of fractures and the damage-induced gouge materials were not considered. The effects of the normal stress and scale effects on dilation (and therefore on aperture and transmissivity) are ignored for simplicity.

3. Numerical study on permeability and REV using UDEC

The studies on the REV and hydraulic permeability tensor using the same site fracture data and considering correlated fracture aperture and trace length is reported in Ref. [5], without stress effect. Since the REV size and the definitions of permeability ellipse (tensor) and error estimation criterion as defined in Ref. [5] are needed to study the stress effects, these findings are briefly presented here.

The geometric parameters for generating fracture network realizations are based on the field mapping results of a site characterization at the Sellafield area, Cambria, UK, as reported in Refs. [45,46] and used in Refs. [4,5]. The basic information of the identified four sets of fractures is shown in Table 1.

The fracture trace lengths follow a truncated power law distribution, with a calculated fractal dimension of 2.2 and a density of 4.6 m^{-2}, respectively. The minimum and maximum detected trace lengths are 0.5 and 250 m, respectively. The orientations of fractures are assumed to follow a Fisher distribution and then the Monte Carlo method is used to generate the trace lengths and the orientations of fractures. The locations of the fractures follow a Poisson process that is the most commonly used

Table 1
Fracture parameters used for discrete fracture network (DFN) generation [4,5,45,46]

Joint set	Dip/dip direction	Fisher constant, K	Fracture density (m^{-2})	Mean trace length (m)
1	8/145	5.9	4.6	0.92
2	88/148	9.0	4.6	0.92
3	76/21	10.0	4.6	0.92
4	69/87	10.0	4.6	0.92

assumption in DFN simulations [4,5]. These geometric parameters of fractures serve only as data sources for generations of DFN realizations for generic studies of hydro-mechanical simulations, not necessarily reflect the actual site conditions.

The log-normal distributions of the hydraulic apertures in the fractured rocks are partially validated by results of a hydraulic test calibration reported in Refs. [21,22]. In this study, hydraulic aperture is log-normally distributed with a mean value of 65 μm and standard deviation of $b=1$. Apertures are correlated with fracture trace lengths through Eq. (14). To avoid the boundary effect, a sufficiently large 'parent' DFN model of 300 m × 300 m size was first generated using Monte Carlo simulations as mentioned in Ref. [5]. Fracture apertures are generated following Eq. (14) and then assigned to fractures in the DFN according to their trace length.

The equivalent permeability tensor, k_{ij}, is calculated from Darcy's law for the equivalent anisotropic and homogeneous porous media, considering flow only in fractures. The other relevant properties of water at a room temperature of 20 °C are a viscosity of 0.001 (Pa s) and a density of 1000 (kg/m^3). As no temperature change is considered and water is assumed to be incompressible in this numerical experiment, the viscosity and density of water do not change during the numerical test.

An average permeability matrix $\bar{k}_{ij}$ of the rotated DFN models is calculated by averaging the projected permeability values on the reference axes (rotation angle, $\alpha=0$) from all rotated permeability components, given as

$$\bar{k}_{ij}=\frac{1}{N}\sum_{1}^{N}k_{pq}^{\alpha}a_{ip}a_{jq}, \tag{15}$$

where N denotes the number of rotations, a_{ip} and a_{jq} are directional cosines, and k_{pq}^{α} is the calculated permeability in each rotated model at direction α. Then $\bar{k}_{ij}$ was transfered to the pertinent rotation angles ($\bar{k}_{ij}(\alpha)$) [5,47]. The average permeability matrix $\bar{k}_{ij}$ thus calculated using Eq. (15) represents a measure of approximation to an ideal ellipse of the permeability in 2D.

The calculated normalized mean square error as used in Ref. [5] shows the goodness of fit between $\bar{k}_{ij}(\alpha)$ and $k_g(\alpha)$ of the calculated directional permeabilities, which are denoted as the rotated average and the actual values calculated for the directional permeabilities:

$$\mathrm{RMS}_{\mathrm{Norm}}=\frac{2}{K_1+K_2}\sqrt{\frac{1}{N}\sum_{1}^{N}\left[k_{\mathrm{g}}(\alpha)-\bar{k}_{ij}(\alpha)\right]^2}, \tag{16}$$

where N is the number of the rotated DEM models, and K_1 and K_2 are the major and minor principle permeability values.

The permeability of a DFN model can be approximated by a tensor if an ellipse can be fitted to the calculated directional permeabilities when plotted as $1/\sqrt{k}$ on a polar diagram [5,47]. If the values of $1/\sqrt{k}$ do not approximate an ellipse, then a symmetric permeability tensor does not exist at that model size. The model size then needs to be enlarged for continued flow simulations until an ellipse of directional permeabilities can be established and the model size is then the hydraulic REV size of the fracture rocks.

The size of the hydraulic REV for this study, as established in Ref. [5], is 20 m × 20 m, with an acceptable coefficient of variance 20%, with a large numbers of realizations and a mean square error 15% in the calculated directional permeabilities.

4. DEM study on stress effect on permeability

In this section, the results of applying different ratios of horizontal/vertical stresses on the DEM models for their effects on permeability and fluid flow patterns are examined, with the DEM models of the hydraulic REV size, as described in Section 3.

4.1. The DEM model establishment

The field and empirical studies have indicated that the ratio of horizontal to vertical in situ rock stresses in subsurface, K, is greater than unity and varies a range up to five and a half [48]. On the other hand empirical and analytical studies have shown that such a stress ratio, at certain depths, varies in special ranges depending on the geological history of the region concerned, structures, mechanical properties of rock and interaction with other agents such as water [49].

In this study we chose the stress ratio in a range of 1–5, with the vertical stress fixed at 5 MPa in order to examine normal and shear deformability of fractures in the DEM models, and compare our results with the results reported in Ref. [4].

Fig. 4 shows the schematic generic boundary conditions for calculation of permeability changes under various applied stresses for the DEM models at a zero rotation angle. For rotated DEM models, the corresponding stress tractions across and along the boundary of the rotated models are first calculated and applied according to the applied principal stress field on the DEM models at reference axis, and then a permeability test is considered. Each DFN model contains about 27,000 small rock blocks that were treated as linear, isotropic, homogeneous, elastic and impermeable materials and subdivided with about 62,000 constant-strain triangle finite-difference elements. Variation in hydraulic behavior of fractures such as opening, closure, sliding and dilation were controlled by incorporating the relative motions and blocks and the fracture constitutive model with a step-wise non-linear normal stress–normal closure relationship to approximate a hyperbolic normal displacement–normal stress behavior, as described in Section 2.1, and a Mohr–Coulomb type of elasto-perfectly plastic shear behavior.

The friction angle and dilation angle of fractures were defined as 24.9° and 5.0°, respectively, and the critical shear

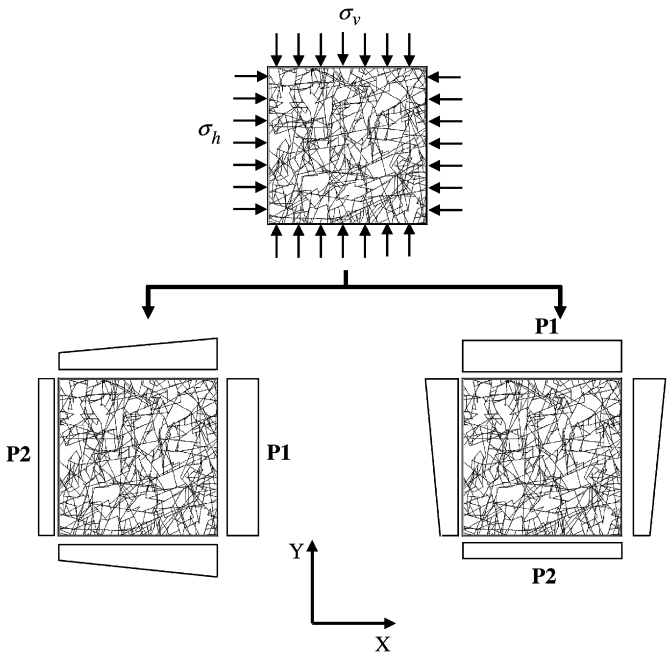

Fig. 4. Application of stress boundary conditions and calculation of equivalent permeability components in the x- and y-directions for the models at reference axis.

displacement for dilation was assumed to be 3 mm. The maximum aperture value by dilation is assumed to be 10 times of residual aperture value for each fracture [4,50].

4.2. Effect of stress ratio on permeability

Fig. 5 shows the variation of the diagonal permeability components k_{xx} and k_{yy} of different rotated DFN models of 20 m × 20 m in size from a no-stress condition to stress conditions of different stress ratios ($K = 1, 3, 4, 5$) when aperture is log-normally distributed with second moment of 1 and correlated with fracture trace length, indicated by legend Ap.Correlated_Rot. For comparison, the results of the models with uniform aperture distribution with DFN size of 5 m × 5 m (directly taken from [3,4]) are also shown, as indicated by legend Ap.Constant_Rot.

With increasing stress ratio from no stress condition ($K=0$) to $K=1$, permeability components for all the rotated models decrease with a factor of one, mainly due to the pure normal closures of fractures under normal stresses without shear. The calculated off-diagonal permeability components show differences of some order of magnitudes compare with the diagonal terms. Therefore the main flow pass is in the direction parallel with hydraulic gradient as can be seen in Figs. 10 and 11. However, at the same applied stress level, when fracture aperture is assumed to be constant in the DEM model [4], overall permeability decreases by two orders of magnitude. The reason for such significant difference between the constant and correlated aperture distributions is that, when the fracture aperture is log-normally distributed and correlated with fracture trace length, the large number of small fractures with small

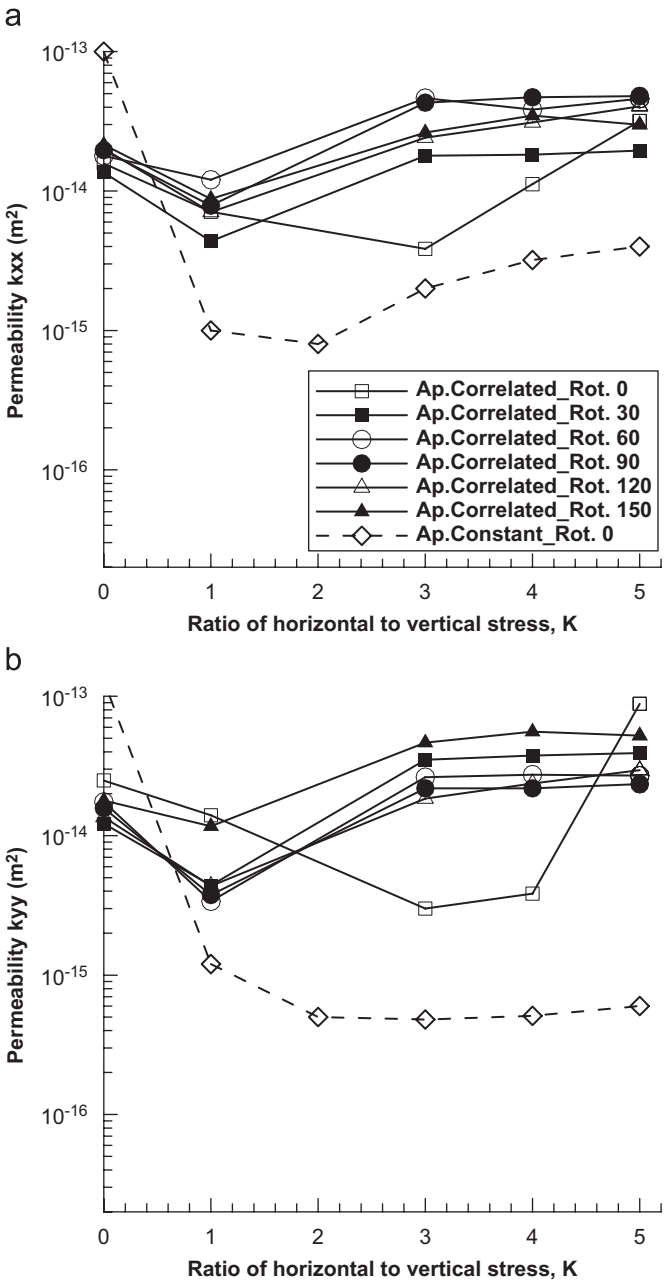

Fig. 5. Permeability components k_{xx} (a) and k_{yy} (b) changes with increasing stress ratios for different rotated DFN models with 20 m × 20 m size when aperture is log-normally distributed and correlated with fracture trace length (Ap.Correlated_Rot.) and also the results of the models with uniform aperture distribution with DFN size of 5 m × 5 m (Ap.Constant_Rot.) taken from [3,4].

aperture values may reach their residual aperture values but some large fractures with much higher initial aperture values remain far from being at residual state and are still highly conductive, so that the overall reduction of permeability of fracture system becomes less compared with the uniform aperture case. When normal stiffness of fracture is scale and stress dependent (Eq. (13)), with increasing of initial aperture (h_i), larger fracture becomes stiffer at lower applied stress conditions (cf., Fig. 3). Therefore under the same stress condition, larger fractures

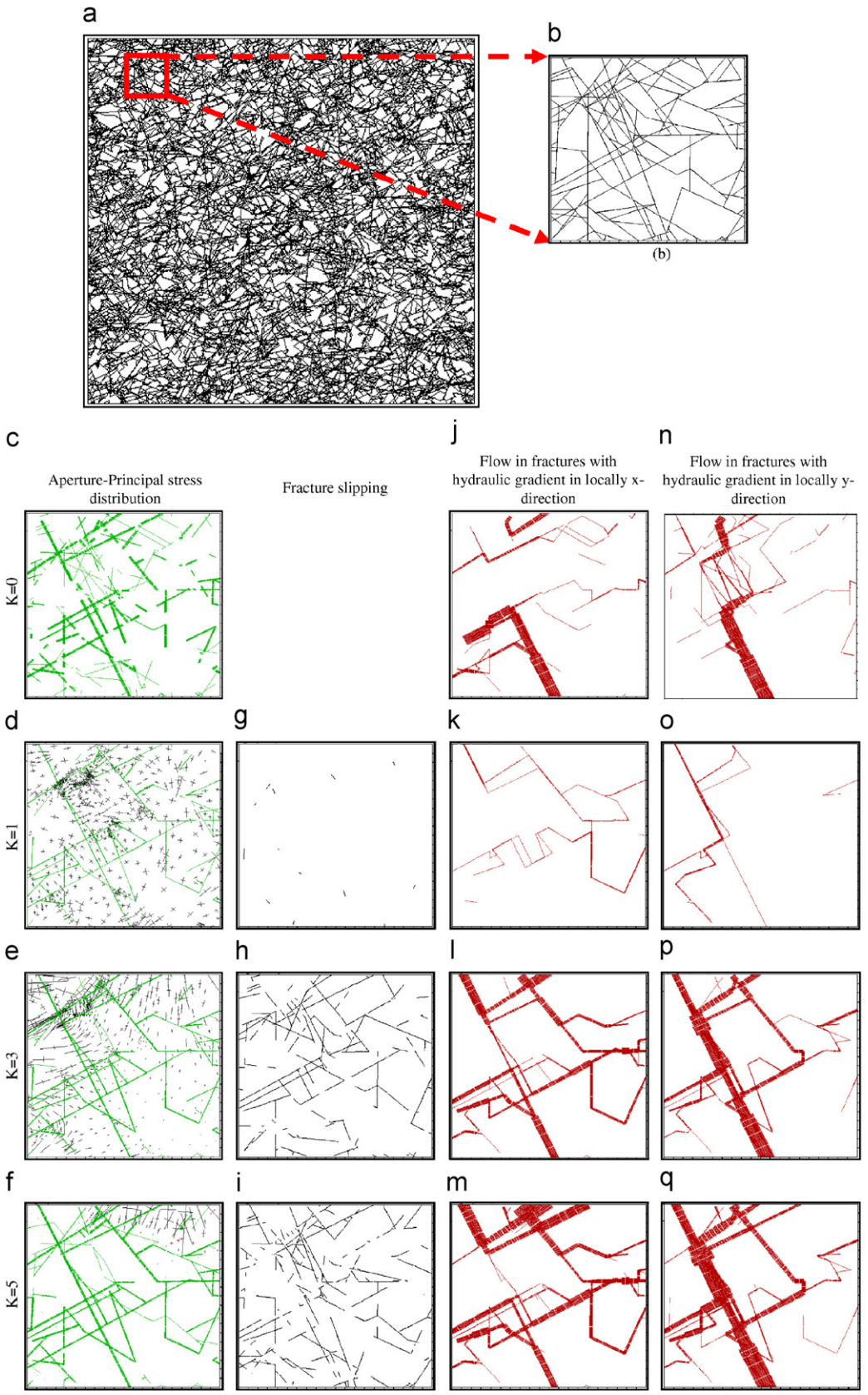

Fig. 6. The DFN model with 20 m × 20 m size at 120° rotation angle (a), extracted a model with 2 m × 2 m in size (b), aperture changes (thickness of the lines) and principal stress vectors (c–f), region of fractures undergoing slipping (g–i), fluid flow rates in the x-direction (j–m) and y-direction (n–q) when no stress applied or stress ratios are $K = 1$, 3 and 5 for the extracted DEM model with 2 m × 2 m in size. Each line indicates the aperture of 40 μm and the maximum aperture presented is 200 μm in (c–f). Also each line represents flow rate of 2×10^{-8} m^3/s in (j–q).

keep larger remaining apertures or transmissivities to conduct fluid flow, even when the smaller fractures may be virtually closed. When stress ratio is increased up to $K = 3$ or higher, most of the fractures will experience shear dilation, which cause continued increase of overall flow rates of the DEM models, and formation of channeled flow paths and changes in the overall permeability. The key factor for channeling and shear failure is the relative orientation of fractures with respect to the stress directions, besides the adopted shear strength criterion and associated properties such as stiffness, friction angle and cohesion. In the DEM models with zero rotation angle (at reference axis), due to the dominant sub-vertical and sub-horizontal orientations of fractures (Table 1), which are parallel with boundary stress directions, most of the fractures are in compression without shear failure, and therefore the overall permeability continue to decrease, until K value is higher than 3 (Fig. 5). For rotated DEM models, shear-induced increase of permeability by dilation can starts at rather low K values (about $K = 1$) (Fig. 5) due to the development of shear dilation in the fractures due to the rotation-induced change of fracture orientation. With a stress ratio up to $K = 5$, most of the fractures, including the large fractures of initial higher aperture values, experience shear dilation in all rotated models, therefore the overall permeability of the rotated DFN models increase rapidly, by a factor of three compared with the no-stress case.

To support the above interpretation, Fig. 6a shows a DFN model with 20 m × 20 m size at a rotation angle of 120°, from which we extracted a model with 2 m × 2 m in size (Fig. 6a) for showing detailed results of aperture changes (thickness of the lines) and principal stress vectors (Fig. 6c–f), fractures undergoing slipping (Fig. 6g–i), fluid flow rates in the x-direction (Fig. 6j–m) and in the y-direction (Fig. 6n–q) with no stress condition ($K = 0$) and stress conditions of stress ratios $K =$ 1, 3 and 5, respectively. When a hydrostatic stress ($K = 1$) is applied, most fractures experience closure without shear except at a few isolated fracture intersections (Fig. 6g) and principal stress pattern is roughly uniformly distributed (Fig. 6d), with fluid flow conducted by some large scale fractures or fracture clusters (Fig. 6k and o). When the stress ratio is increased to $K = 3$ and 5, fracture apertures increase more widely by shear induced slipping and dilation of fractures (Fig. 6h and i) caused by rotated and concentrated stresses at fracture intersections (Fig. 6e–f). Fluid flow rate distributions at different applied stress ratios in the DEM models (Fig. 6j–q) show that beside the connectivity of fracture network, a small number of long fractures with large initial aperture values always remain conductive in all stress conditions and has a significant influence on the overall permeability and flow patterns, particularly when fluid flows in the y-direction (Fig. 6i–q). These large conducive features are dominant major flow pathways and influence the overall permeability of DEM models significantly (Fig. 6l, m, p and q).

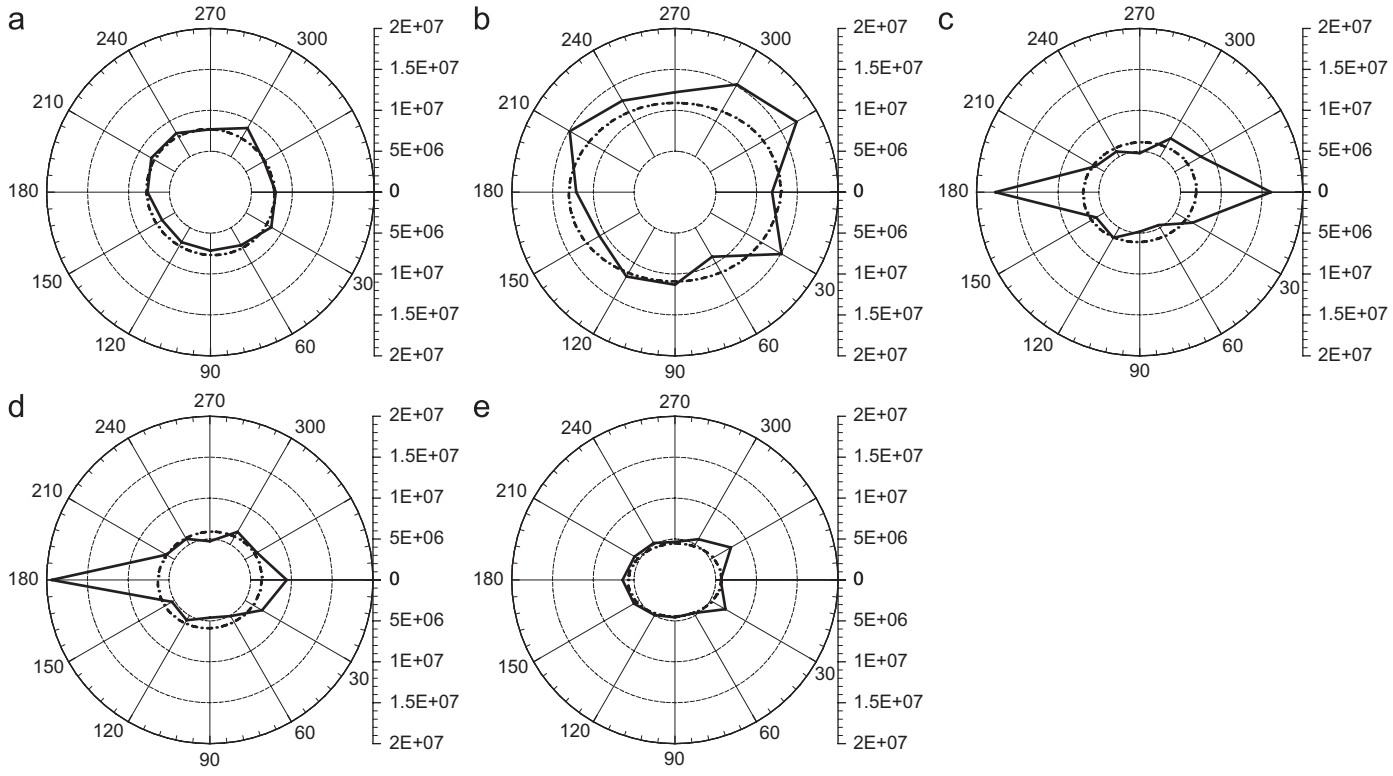

Fig. 7. Directional permeability contours and mean square errors for DFN models at stress ratio: (a) initial no stress condition, (b) $K = 1$, (c) $K = 3$, (d) $K = 4$ and (e) $K = 5$ (expressed in $1/k^{1/2}$ (m^{-1})).

4.3. Evaluation of permeability tensor and flow pattern changes with different stress ratios

Fig. 7 shows the calculated reciprocal values of the directional permeabilities for the no-stress condition and $K = 1$, 3, 4 and 5. Dashed lines represent the mean values of $1/\sqrt{\bar{k}_{ij}(\alpha)}$, and solid lines represent the calculated directional permeability values, $1/\sqrt{k_g(\alpha)}$, as described in Section 3. Both are plotted in a polar coordinate system. The contours of the directional permeabilities are plotted in the same scale, and larger contour sizes represent lower permeability values. Below each figure the applied stress ratio (K) on the DEM models and the calculated normalized mean square error using Eq. (16) is presented.

At the initial no-stress condition $K = 0$, a permeability ellipse can be approximated with an accepted value of $\mathrm{RMS}_{\mathrm{Norm}} = 15\%$ for a tensor representation with a REV size of $20\,\mathrm{m} \times 20\,\mathrm{m}$ (Fig. 7a). Fig. 8 shows the fluid flow patterns with flow in the local x-directions under no stress condition for rotated DFN models. The major flow pathways are more oriented in the direction parallel with hydraulic gradient. The large conductive features mainly oriented in the sub-vertical direction as shown in Fig. 9, still have certain influence on overall flow pattern for the rotated models, as demonstrated by the slightly larger permeability in the vertical directions (shown as slight shrinkage of the ellipse in 90° and 270° directions in Fig. 7a). However, the overall permeability is quite homogeneous with a good fit to a permeability ellipse for the no-stress condition case.

When a hydrostatic stress field is applied ($K = 1$), the values of the permeability components decrease, as indicated by the enlarged directional permeability contour in Fig. 7b, especially in the 30° rotation direction. A mean square error of $\mathrm{RMS}_{\mathrm{Norm}} = 0.31$ still cannot justify the

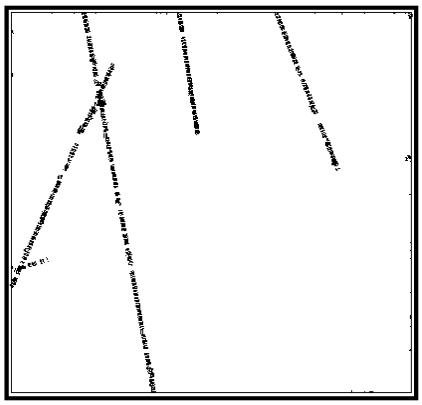

Fig. 9. Locations of large fractures in the DFN model at reference axes (zero rotation) with more than 150 μm initial hydraulic aperture.

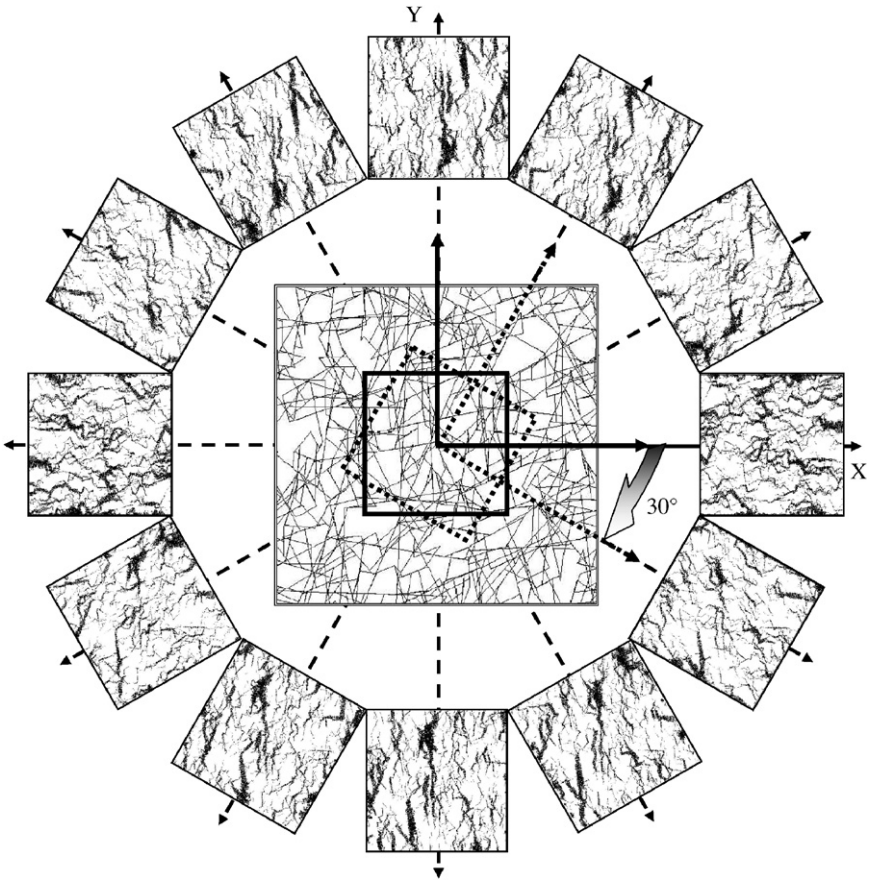

Fig. 8. Fluid flow patterns in the rotated x-direction for rotated DFN models at the initial condition (without stress). Each line indicates the flow rate of $2 \times 10^{-8}\,\mathrm{m}^3/\mathrm{s}$ and an example of extracted rotated DFN models through the large-scale parent model (in center part of the figure).

existence of a permeability tensor. Flow is channeled mainly along the clustered fractures sub-oriented roughly in parallel or in small angles with the local direction of the hydraulic gradient (Figs. 10b–f and 11b–f). Since $K=1$, no significant shear failure is induced in fractures and the flow paths are dominated by the localized clusters of fractures. The overall permeabilities of the DEM models are reduced because that compression is the dominating mode of loading state (see Fig. 6d, g, k and o)

At the higher applied stress ratios $K=3$ and 4 (Fig. 7c and d), shear dilation of fractures dominates the overall permeability behaviors of the rotated DEM models (except the non-rotated DEM models along the original axis as shown also in Figs. 10g and 11g) and the directional

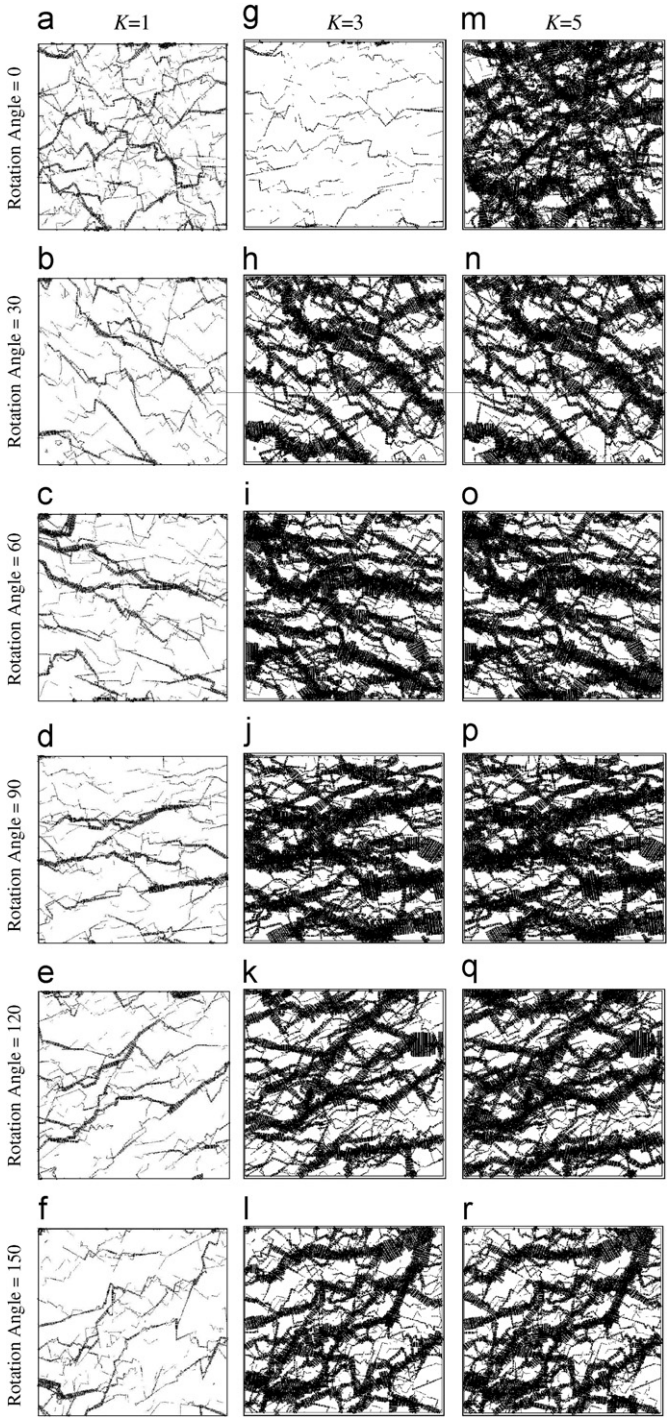

Fig. 10. Fluid flow patterns for rotated DFN models when fluid flows parallel to the horizontal stress with $K=1$ (a–f), $K=3$ (g–l) and $K=5$ (m–r). Each line indicates the flow rate of $2\times10^{-8}\,m^3/s$.

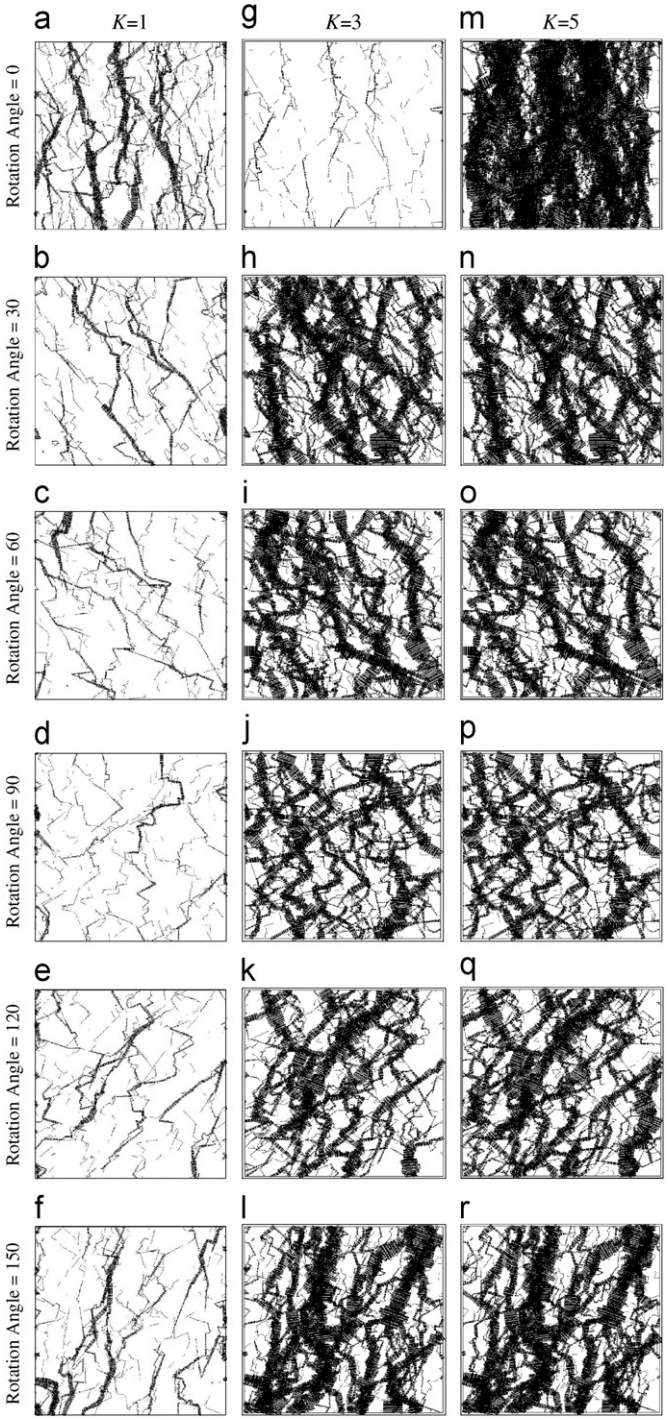

Fig. 11. Fluid flow patterns for rotated DFN models when fluid flows perpendicular to the horizontal stress with $K=1$ (a–f), $K=3$ (g–l) and $K=5$ (m–r). Each line indicates the flow rate of $2\times10^{-8}\,m^3/s$.

permeability contours are more inclined horizontally due to effects of shear failure and dominating sub-vertically oriented main fractures and fracture clusters. The directional premeabilities increased significantly in the sub-vertical directions, and much decreased in the sub-horizontal direction, as indicated by the much-reduced reciprocal of the vertical permeability and enlarged reciprocal of the horizontal permeability in Fig. 7c and d, respectively. The fluid flow in the rotated models was dominated in their respective local x and y-directions as shown in Figs. 10h–l and 11h–l, with significant flowrate increase in their local x- and y-directions. In these DEM models, a combination of shear dilation of fractures (even of small sizes) and larger fractures of higher aperture values that remain open, increase the overall fracture network permeability in the particular direction defined by the shear stress component. The dominance of the larger fractures or main clusters of smaller fractures is not as strong as in the hydrostatic stress state case. At these stress states, $K=3$ and $K=4$, calculated mean square errors are 0.52 and 0.43, respectively, and acceptable permeability ellipses cannot be approximated.

When $K=5$, with the generated fracture orientations and assigned friction angle and dilation angle values, most of fractures in DFN models experience shear dilation with much increased overall permeability and the overall flow behavior of the DEM models becomes more homogeneous, as indicated by the general reduction of the reciprocal values of directional permeabilities in Fig. 7e. Although a perfect ellipse is still not possible, the calculated mean square error is $\mathrm{RMS}_{\mathrm{Norm}}=0.22$, very close to be a permeability tensor for practical applications. At this stress state condition ($K=5$), patterns of the dominating flow pathways are similar to that with $K=3$, but extent of channeling become more significant due to the continued increase of the shear dilation of fractures (although with smaller gradient). The overall permeability increases accordingly (Figs. 10m–r and 11m–r). The contribution of smaller fractures becomes more significant due to the continued development of shear dilation as induced by the stress ratios. Therefore the main directions of fluid flow pathways correspond to the overall shear stress directions.

The above results indicate an important aspect of stress effect on permeability change, i.e. the stress field may cause or destroy the existence of an equivalent permeability tensor for certain fracture systems depending on applied stress ratios, geometric characteristics of the fracture system and the mechanical properties of fractures.

5. Discussion and conclusion

The stress effect on permeability magnitude, existence of equivalent permeability tensor and fluid flow pathways in DEM models representing a 2D fractured rock mass was studied. A model for the prediction of normal deformability behavior of fractures is developed when log-normally distributed fracture aperture is correlated with the trace length, following a power law distribution. This correlation enables us to study both the scale and the stress effects of fractures on the overall hydro-mechanical behaviors of fractured rocks, considering the coupling between spatial variation of geometric characteristics and mechanical behaviors of rock fractures.

The results show that this coupling has significant impacts on the stress-induced flow pattern and permeability changes of fractured rocks. With increasing the ratio of applied horizontal to vertical stresses (K) on the DEM models, from initial no stress condition to a hydrostatic stress state $K=1$, permeability components for all the rotated DEM models decrease, mainly due to the hyperbolic behavior of fracture deformability without shear failure. The large fractures of higher permeability values in the model play a major role for localized flow patterns and higher permeability values compared with the constant aperture cases as studied in Ref. [4], showing differences of two orders of magnitude in equivalent permeabilities. When stress ratio increases to $K=3$ or higher, contribution of shear dilation of the smaller fractures becomes the main reason for continued flow channeling and increase of overall DEM model permeability. In addition, the relative orientation of fractures with respect to the shear stress direction, initial aperture, friction angle and dilation angle of the fractures are important factors for the occurrence of shear failure of fractures, therefore the existence of equivalent permeability tensor. This is demonstrated, in Figs. 7c and d, that in the DEM models with zero rotation angle (at reference axis), even at a high values of stress ratio ($K=3$ and 4) some of the large fractures in the compression state without shear failure are still conductive and contribute to overall permeability.

The results show that the correlation between fracture size and its hydraulic permeability is an important issue affecting the conceptualization and formulation of DEM models for fractured rocks as equivalent continua. The smaller number of large fractures of higher aperture values dominates the flow pattern and change of overall permeability of the fracture systems to a significant extent, especially at smaller magnitude of stress ratios. Only under higher stress ratios ($K=3$ or higher in the cases studied here) the dilation caused by shear failure of large portion of smaller fractures starts to play a more important role in flow channeling and change of permeability. It is the main reason why network permeability decreases much more drastically when correlation between fracture trace length and aperture has not been considered.

In this numerical modeling only the connected fractured are included for flow analysis, therefore all flow channels are continuous but can be very tortuous as shown also in Fig. 8. However, stress-induced channeling effect occurs only when high value of stress ratio ($K=3$ or higher) is applied (Figs. 10h–r and 11h–r).

The calculated directional permeabilities with different applied stress ratios show that a permeability tensor established without considering stress effect may lead to

significant misunderstanding of the overall hydraulic behavior of fractured rocks that are generally under stressed conditions. The permeability tensor may exist at no stress condition, but may be destroyed or re-established with different in situ stress conditions with different permeability values, as demonstrated in Fig. 7. Therefore, adequate characterization of the fracture system geometry, mechanical behaviors and properties of individual fractures and in situ stress condition (and its change due to engineering or tectonic causes) are key issues for more realistic understanding and quantification of permeability field and its evolution. This presents a major challenge to site characterization and numerical modeling of subsurface engineering works, especially oil or geothermal reservoir fields and nuclear waste repositories.

The results demonstrate, once again, that the correlations between geometric paramaters of fractures is an important issue in not only the numerical models but also practical rock engineering. Ignorance of such correlations, especially impact of fracture size, may lead to significant uncertainties in the estimations of scale effects of equivalent properties such as permeability variation, existence of permeability tensor and interpretation of fliud flow patterns in fractured rocks. The results demonstrate that when fracture aperture is correlated with fracture trace length, the overall permeability of the model can be controlled by fewer numbers of large fractures of higher aperture values even without stress effects considered.

Our study is a generic study aimed at establishing a general stochastic approach for studying stress-scale effects on permeability of fractured rock masses, using distributed geometric parameters of fracture systems. Care should be taken for reliable fracture system characterization if such an approach is applied for site-specific investigations. The validity of conclusions drawn are restricted to the provided distribution functions for fracture system parameters and mechanical properties of rock matrix and fractures.

In this study we assumed that the hydraulic apertures (or transmissivity) of fractures are log-normally distributed with second moment of $b = 1$ and correlated to the power law distribution of fracture trace length. Similar algorithm can be established with different distribution functions of gemetrical parameters of fractures. For instance the impact of large value of second moment that makes the aperture pattern more scattered, and also when fracture aperture is distributed independently regardless of fracture trace length, are planned for future studies.

It should also be noted that the mechanical properties of rock matrix and fractures used in this study were site-specific data, and we did not run sensitivity studies on these properties, since our focus is on stress-scale effects on fracture systems of correlated geometric parameters, not mechanical properties. Therefore, effects of the mechanical properties were not systematically assessed and not considered in the general conclusions.

During the normal loading, and also shear failure processes in fractures, gouge materials may be produced. In general, production of the gouge materials during the coupled shear-flow tests increases the ratio of mechanical aperture/hydraulic aperture, and reduces the permeability of single fractures in relation to the predicted effect of dilation [51,52]. However, the development of constitutive models considering effect of gouge materials on transmissivity of fractures needs more data support from experiments, and is beyond the scope of this study.

The current study is a generic study limited to 2D analysis since the main object of this study is to highlight the impact of correlation between aperture and trace length of fractures on hydraulic behaviors of fractured crystaline rocks when effect of stress fields is considered. The results and conclusions are also subject to validity of constitutive models and assumed hydro-mechanical properties of individual fractures. We adopted these simple models for establishing a useful numerical approach and demonstrate the importance of large fractures and stress effect for continued fundamental researches. Similar studies could be carried out in 3D, in principle, but considerable improvement on data support and computational efficiency are required.

Using the truncated distributions of initial aperture and trace length of fractures makes special source of uncertainty. However, because of limitations in measuring the geometric parameters and mechanical properties of each fracture in the field, using the truncation distribution cannot be avoided, as discussed and explained more explicitly in Ref. [5].

Acknowledgements

The financial support by the Ministry of Science, Research and Technology of Islamic Republic of Iran is greatly acknowledged. The authors also thank Prof. R.W. Zimmerman of the Engineering Geology and Geophysics Group at KTH for help and fruitful discussions.

References

[1] Rutqvist J, Stephansson O. The role of hydromechanical coupling in fractured rock engineering. Hydrogeol J 2003;11:7–40.
[2] Priest SD. Discontinuity analysis for rock engineering. London: Chapman & Hall; 1993.
[3] Min KB, Jing L, Stephansson O. Determining the equivalent permeability tensor for fractured rock masses using a stochastic REV approach: Method and application to the field data from Sellafield, UK. Hydrogeol J 2004;12(5):497–510.
[4] Min KB, Rutqvist J, Tsang CF, Jing L. Stress-dependent permeability of fractured rock masses: a numerical study. Int J Rock Mech Min Sci 2004;41(7):1191–210.
[5] Baghbanan A, Jing L. Hydraulic properties of fractured rock masses with correlated fracture length and aperture. Int J Rock Mech Min Sci 2007;44(5):704–19.
[6] Bandis SC. Experimental studies of scale effects on shear strength and deformation of rock joints. PhD thesis, University of Leeds, UK, 1980.
[7] Oda M. An equivalent continuum model for coupled stress and fluid flow analysis in jointed rock masses. Water Resour Res 1986;22(13):1845–56.

[8] Chen M, Bai M. Modeling stress-dependent permeability for anisotropic fractured porous rocks. Int J Rock Mech Min Sci 2005; 35(8):1113–9.
[9] Oda M, Hatsuyama Y, Ohnishi Y. Numerical experiments on permeability tensor and its application to jointed granite at Stripa Mine, Sweden. J Geophys Res 1987;92(B8):8037–48.
[10] Ouyang Z, Elsworth D. Evaluation of groundwater flow into mined panels. Int J Rock Mech Min Sci Geomech Abstr 1993;30(2):71–9.
[11] Zhang X, Sanderson DJ, Harkness R, Last NC. Evaluation of the 2D permeability tensor for fractured rock masses. Int J Rock Mech Min Sci 1996;33(1):17–37.
[12] Zhang X, Sanderson DJ. Effect of stress on the two-dimensional permeability tensor of natural fracture networks. Gephys J Int 1996;125:912–24.
[13] Zhang X, Sanderson DJ. Numerical study of critical behavior of deformation and permeability of fractured rock masses. Marine Pet Geol 1998;15:535–48.
[14] Zhang X, Powrie W, Harkness R, Wang S. Estimation of permeability for the rock mass around the Shiplocls of the Three Gorges Project, China. Int J Rock Mech Min Sci 1999;36:381–97.
[15] Indraranta B, Ranjith PG, Gale W. Single phase water flow through rock fractures. Geotech Geol Eng 1999;17:211–40.
[16] Zhang X, Sanderson DJ. Evaluation of instability in fractured rock masses using numerical analysis methods: effect of fracture geometry and loading direction. J Geophys Res 2001;106(B11):26671–87.
[17] Lee SD, Moon HK. A study on the groundwater flow and grouting around underground openings based on stress-dependent discrete joint network analysis. In: Ohnishi A, editor. Proceedings of 3rd internationalARMS symposium, Balkema, 2004. p. 1107–10.
[18] Blum P, Mackay R, Riley MS, Knight JL. Performance assessment of a nuclear repository: upscaling coupled hydro-mechanical properties for far field transport analysis. Int J Rock Mech Min Sci 2005;42: 781–92.
[19] Margolin G, Berkowitz B, Scher H. Structure, flow, and generalized conductivity scaling in fracture networks. Water Resour Res 1998; 34(9):2103–21.
[20] de Dreuzy JR, Davy P, Bour O. Hydraulic properties of two-dimensional random fracture network following a power law length distribution. 2. Permeability of networks based on lognormal distribution of apertures. Water Resour Res 2001;37(8):2079–95.
[21] Dverstop B, Andersson J. Application of the discrete fracture network concept with field data: Possibilities of model calibration and validation. Water Resour Res 1989;25(3):540–50.
[22] Cacas MC, Ledoux E, de Marsily G, Tillie B, Barbreau A, Durand E, et al. Modeling fracture flow with a stochastic discrete fracture network: calibration and validation. 1. The flow model. Water Resour Res 1990;26(3):479–89.
[23] Niemi A, Kontio K, Kuusela-Lahtinen A. Hydraulic characterization and upscaling of fracture networks based on multi-scale well test data. Water Resour Res 2000;36(12):3481–98.
[24] Öhman J, Niemi A. Upscaling of fracture hydraulics by means of an oriented correlated stochastic continuum model. Water Resour Res 2003;39(10).
[25] Öhman J, Niemi A, Tsang CF. A regional-scale particle-tracking method for nonstationary fractured media. Water Resour Res 2005; 41(3).
[26] Öhman J, Niemi A, Tsang CF. Probabilistic estimation of fracture transmissivity from wellbore hydraulic data accounting for depth-dependent anisotropic rock stress. Int J Rock Mech Min Sci 2005;42(5–6):793–804.
[27] Vermilye JM, Scholz CH. Relation between vein length and aperture. J Struct Geol 1995;17(3):423–34.
[28] Hatton CG, Main IG, Meredith PG. Non-universal of fracture length and opening displacement. Nature 1994;367:160–2.
[29] Renshaw CE, Park JC. Effect of mechanical interactions on the scaling of fracture length and aperture. Nature 1997;386:482–4.
[30] Itasca Consulting Group Inc. UDEC user's guide, version 4.0. Minneapolis, MN, 2004.
[31] Iwai K. Fundamental of fluid flow through a single fracture. PhD thesis, University of California, Berkeley, 1976.
[32] Goodman RE. Methods of geological engineering in discontinues rocks. New York: West Pub; 1976.
[33] Bandis SC, Lumsden AC, Barton NR. Fundamental of rock joint deformation. Int J Rock Mech Min Sci 1983;20:249–68.
[34] Raven KG, Gale JE. Water flow in a natural rock fracture as a function of stress and sample size. Int J Rock Mech Min Sci 1985; 22:251–61.
[35] Yoshinaka R, Yabame T. Joint stiffness and deformation behavior of discontinues rock. Int J Rock Mech Min Sci 1986;23(1): 19–28.
[36] Evans KF, Cornet FH, Hashida T, Hayashi K, Ito T, Matsuki K, et al. Stress and rock mechanics issues of relevance to HDR/WDR engineered geothermal systems: review of developments during the past 15 years. Geothermics 1999;28:455–74.
[37] Pyrak-Nolte LJ, Morris JP. Single fractures under normal stress: the relation between fracture specific stiffness and fluid flow. Int J Rock Mech Min Sci 2000;37:245–62.
[38] Lee HS, Cho TF. Hydraulic characteristics of rough fractures in linear flow under normal and shear load. Rock Mech Rock Eng 2002;35:299–318.
[39] Gentier S, Hopkins D. Mapping fracture aperture as a function of normal stress using a combination of casting, image analysis and modeling. Int J Rock Mech Min 1997;34:3–4.
[40] Esaki T, Du S, Mitani Y, Ikusada K, Jing L. Development of a shear-flow test apparatus and determination of coupled properties for a single rock joint. Int J Rock Mech Min Sci 1999;36: 641–50.
[41] Olsson R, Barton N. An improved model for hydromechanical coupling during shearing of rock joints. Int J Rock Mech Min Sci 2001;38:317–29.
[42] Jiang Y, Xiao J, Tanabashi Y, Mizokami T. Development of an automated servo-controlled direct shear apparatus applying a constant normal stiffness condition. Int J Rock Mech Min Sci 2004; 41(2):275–86.
[43] Bandis SC, Barton NR, Christianson M. Application of a new numerical model of joint behavior to rock mechanics problems. In: Proceedings of international symposium on fund rock joints, Bjorkliden, Sweden, 1985. p. 345–456.
[44] Jaeger JC, Cook NGW, Zimmerman RW. Fundamentals of rock mechanics. 4th ed. Oxford: Blackwell; 2007.
[45] Nirex. The lithological and discontinuity characteristics of the Borrowdale Volcanic Group at the outcrop in the Craghouse Park and Latterbarrow areas. Nirex Report SA/97/029, Harwell, UK, 1997.
[46] Nirex. Evaluation of heterogeneity and scaling of fractures in the Borrowdale Volcanic Group in the Sellafield area. Nirex Report SA/ 97/028, Harwell, UK, 1997.
[47] Bear J. Dynamics of fluids in porous media. New York: Elsevier; 1972.
[48] Brown ET, Hoek E. Trends in relationships between measured in-situ stresses and depth. Int J Rock Mech Min Sci 1978;15:211–5.
[49] Sen Z, Sadagah BH. Probabilistic horizontal stress ratios in rock. Math Geol 2002;34(7):845–55.
[50] Nirex. Data summary sheets in support of gross geotechnical predictions. Nirex Report SA/97/052, Harwell, UK, 1997.
[51] Makurat A, Barton N, Rad NS, Bandis S. Joint conductivity variation due to normal and shear deformation. In: Proceedings of international symposium on rock joints, Loen, Norway. Balkema, Rotterdam, 1990. p. 535–40.
[52] Olsson R, Barton N. An improved model for hydromechanical coupling during shearing of rock joints. Int J Rock Mech Min Sci 2001;38(3):317–29.